Coupling Substrate-Integrated Waveguides to Increase the Gain Bandwidth of Leaky-Wave Antennas

Miguel Poveda-García, David Cañete-Rebenaque, George Goussetis, *Senior Member, IEEE*, and José Luis Gómez-Tornero, *Senior Member, IEEE*

***Abstract*— A novel technique to increase the pattern bandwidth of substrate-integrated waveguide leaky-wave antennas (SIW LWAs) is proposed. By coupling several SIWs, it is shown that the gain at the desired angle can be kept stable across a wide-frequency band. A systematic design methodology based on a simple transverse equivalent network is presented. Practical coupled-SIW designs with gain exceeding 10 dB and pointing at 30° in the 15-GHz band are reported to validate the theory. Simulation and experimental results demonstrate an enhancement of the half-power gain bandwidth from 2.5% (380 MHz) in the single-SIW design to 9% (1360 MHz) for an LWA composed of three coupled SIWs.**

***Index Terms*— Broadband antennas, frequency beam squint, leaky-wave antennas (LWAs), substrate-integrated waveguide (SIW).**

I. Introduction

FREQUENCY squint is a well-known property of leaky-wave antennas (LWAs), due to their characteristic frequency-scanning behavior [1]. It might be a useful characteristic for particular scenarios such as frequency-modulated continuous-wave radars [2]–[4], or frequency-steered near-field focusing systems [5]. However, the beam squint is an undesired feature which limits the practical bandwidth in important applications such as highly directive point-to-point telecommunication radio links. For this reason, many efforts have recently been placed to design high-gain scanning LWAs with reduced frequency-scanning sensitivity [6]–[15]. Neto *et al.* [6], [7] proposed a nondispersive printed leaky slot line embedded in a circularly symmetric elliptical dielectric lens which focuses the radiated fields to a constant beam direction over a wide-frequency range. However, this solution lacks the simple 2-D structure of planar LWAs. Planar LWAs using metamaterial unit-cells have been proposed to modify the frequency dispersion and reduce the beam squint [8]–[11]. Anisotropic meta-substrates [12] and non-reciprocal ferrite-based metamaterials [13] have also proven beam squint reduction. Finally, active circuits can provide non-Foster dispersion responses for squint-free LWAs operating at an off-broadside angle [14], [15]. In this paper, we describe a totally different technique to improve the gain bandwidth of planar LWAs in substrate-integrated waveguide (SIW) technology. The proposed technique dispenses the need of bulky dielectric lenses, metamaterial unit-cells, anisotropic materials, or active circuits. The novel structure is based on the SIW LWA [16] shown in Fig. 1(a), which is modified by adding extra longitudinally coupled SIWs [17], [18].

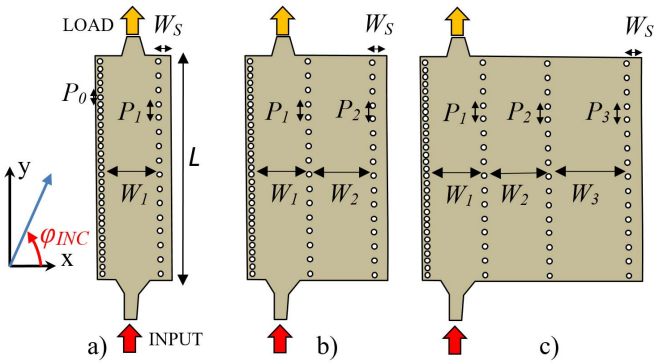

Fig. 1. Scheme of coupled SIW LWA of order. (a) $N = x1$. (b) $N = 2$. (c) $N = 3$.

This coupled SIW LWA topology is inspired by a similar multilayer arrangement used for Fabry–Pérot cavity antennas (FPA) [19]–[25]. The addition of extra coupled FP cavities has demonstrated increased pattern bandwidth (PBW) for high-gain broadside radiation compared to the original single-cavity FPA. In the same manner, in this paper, it is demonstrated for the first time that the high-gain radiation pattern of the single SIW LWA [Fig. 1(a)] can be improved in terms of gain bandwidth at a given off-broadside elevation angle by increasing the number of coupled SIWs. The design theory is based on a simple transverse equivalent network (TEN) which is optimized to satisfy the associated phase resonant condition for the desired angle over a wideband, as described in Section II. Practical examples of coupled SIW LWAs operating at the frequency of 15 GHz and pointing at a 30° angle

Manuscript received October 5, 2017; revised January 14, 2018; accepted March 16, 2018. Date of publication May 9, 2018; date of current version June 4, 2018. This work was supported in part by the Spanish National Project under Grant TEC2013-47037-C5-5-R, and Grant TEC2016-75934-C4-4-R and in part by the Regional Seneca project under Grant 19494/PI/14. *(Corresponding author: Miguel Poveda-García.)*

M. Poveda-García, D. Cañete-Rebenaque, and J. L. Gómez-Tornero are with the Group of Electromagnetism Applied to Telecommunications, Technical University of Cartagena, 30202 Cartagena, Spain (e-mail: miguel.poveda@upct.es; david.canete@upct.es; josel.gomez@upct.es).

G. Goussetis is with the Institute of Sensors Signals and Systems, Heriot-Watt University, EH14 4AS Edinburgh, U.K. (e-mail: g.goussetis@hw.ac.uk).

Color versions of one or more of the figures in this paper are available online at http://ieeexplore.ieee.org.

Digital Object Identifier 10.1109/TMTT.2018.2830396

are presented in Section III, illustrating that higher bandwidth with squint-free condition is obtained as the number of coupled SIWs (N) is increased from 1 to 3. Finally, Section IV reports experimental validation performed on manufactured prototypes, and Section V presents the conclusion.

Previous results presented in [17] and [18] have been improved with the following contributions. First, a polynomial fitting of the TEN components is proposed to reduce the time of optimization. Second, we use the half-power gain bandwidth definition to quantitatively demonstrate the improvement in the antenna bandwidth for the desired scanning angle. Third, detailed description of the optimization process to obtain the highest possible gain bandwidth is explained in section III-B. Finally, experimental demonstration is also reported for the first time in this paper.

II. Design Theory

The structure of the proposed coupled SIW LWA is illustrated in Fig. 1. The original SIW LWA [16] shown in Fig. 1(a) is formed by a single SIW of width W_1 created between a dense row of vias of diameter d and periodicity P_0 acting as totally reflective wall, and a partially reflective sheet (PRS) of vias with similar diameter d and located at a bigger distance P_1 to allow for power leakage. Radiation occurs at the end fringe of the strip of width W_S located at the right side of the SIWs in Fig. 1. A quasi-TE$_{10}$ leaky mode with dispersive complex longitudinal propagation constant $k_y(f)$ can model this continuous radiation along the antenna length

$$k_y(f) = \beta_y(f) - j\alpha_y(f). \tag{1}$$

The antenna length L behaves as a magnetic-current line source that radiates in the form of a fan beam. If low-leakage condition is assumed ($\beta_y \gg \alpha_y$), the elevation angle θ_R [measured from broadside, see Fig. 2(a)] and the 3-dB beamwidth $\Delta\theta$ are related to the leaky-mode phase constant β_y by the following equations [1]:

$$\sin\theta_R(f) \approx \frac{\beta_y(f)}{k_0} = c_0\frac{\beta_y(f)}{2\pi f} \tag{2}$$

$$\Delta\theta_R(f) \approx \frac{1}{\mathrm{L}/\lambda_0 \cos\theta_R(f)} \tag{3}$$

where k_0 is the free-space wavenumber, λ_0 is the free-space wavelength, and c_0 is the speed of light in air. To eliminate the frequency-beam squint, the angle θ_R must be fixed to a constant goal value for all frequencies, so from (2), we obtain a linear dependence with frequency for $\beta_y(f)$ that must be satisfied

$$\theta_R(f) = \theta_{\mathrm{GOAL}} \rightarrow \beta_y(f) = \beta_{y\mathrm{GOAL}}(f) = \frac{2\pi f}{\mathrm{c}_0}\sin\theta_{\mathrm{GOAL}}. \tag{4}$$

To analyze the leaky-mode phase constant dispersion $\beta_y(f)$, a simple TEN along the x-direction proposed in [26] and shown in Fig. 2 can be used.

A T-junction network formed by two series capacitances C_S and a parallel inductance L_P given by Marcuvitz [27] is used to model each row of conducting vias of diameter d and

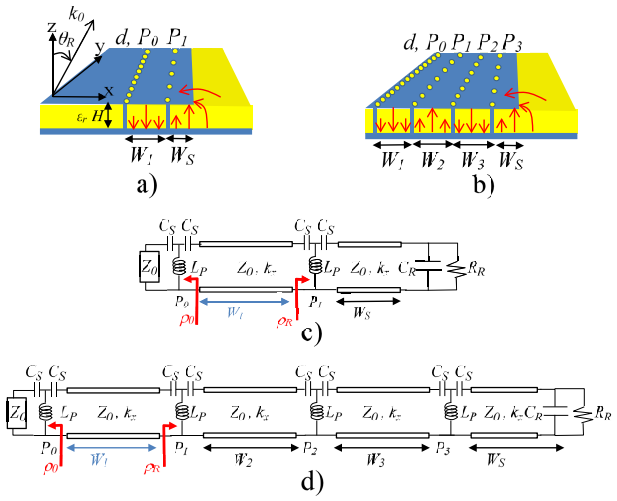

Fig. 2. 3-D view of a coupled-SIW LWA of order. (a) $N = 1$. (b) $N = 3$ and associated TEN. (c) $N = 1$. (d) $N = 3$. Red lines in (a) and (b) represent the fundamental TE leaky-mode electric field distribution.

for any periodicity P. The strip fringe radiation impedance is modeled by a shunt capacitor C_R and a shunt resistance R_R, which values are computed for the SIW host substrate of height H and relative dielectric constant ε_r using Kuester approximation for thin substrates [28]. It must be taken into account that the values for C_S, L_P, C_R, and R_R depend on the internal angle of incidence φ_{INC} shown in Fig. 1(a) [26], which is related to the leaky radiation angle θ_R and phase constant β_y by the Snell equation

$$\sin\varphi_{\mathrm{INC}}(f) = \frac{\sin\theta_{\mathrm{R}}(f)}{\sqrt{\varepsilon_r}} \approx \frac{\beta_y(f)}{\mathrm{k}_0\sqrt{\varepsilon_r}}. \tag{5}$$

For the efficient design of the multicavity SIW LWA, the values of C_S, L_P are first computed for a range of posts periodicity values P using an accurate in-house tool based on the Method of Moments (MoM) [26], and for any fixed incidence angle φ_{INC}. Then a second-degree polynomial fitting is carried out to obtain closed-form expressions for the component values as a function of P

$$L_P(P) = a_L P^2 + b_L P + c_L \tag{6}$$

$$C_S(P) = a_C P^2 + b_C P + c_C. \tag{7}$$

Fig. 3 represents these functions for an internal angle of incidence $\varphi_{\mathrm{INC}} = 19°$, as a function of P in the range from $P = 2$–7 mm, and for a postdiameter $d = 1$ mm. They are compared with MoM results showing good agreement in the full range of values of P. Clearly, the use of closed-form analytical expressions lowers the computational cost needed compared to full-wave MoM analysis. This time reduction is indispensable for the subsequent optimization technique, which needs hundreds of analyses to properly design the distance P between coupling posts for each row of coupling vias.

Next, the SIWs are modeled in the TEN by transmission lines of length Wi, TE characteristic impedance $Z_0 = 1/\omega k_x$ and complex transverse propagation constant $k_x(f)$ related to

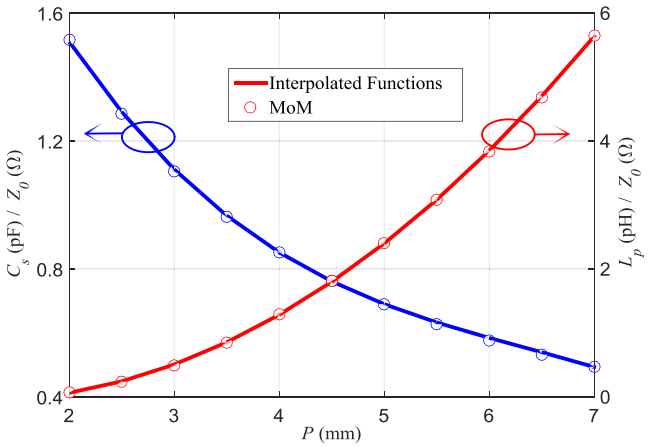

Fig. 3. Variation of C_S and L_P as a function of vias periodicity P and frequency for a fixed incidence angle $\varphi_{\mathrm{INC}} = 19°$, with $d = 1$ mm.

the leaky-mode longitudinal constant $k_y(f)$ (1) by

$$k_x(f) = \sqrt{k_0^2 \varepsilon_r - k_y(f)^2} = \beta_x(f) + j\alpha_x(f). \tag{8}$$

Under low-leakage conditions ($\beta_y \gg \alpha_y$) and using (2), (8) can be rewritten as a function of frequency and the angle θ_R

$$\mathrm{k_x}(f) \approx \beta_{\mathrm{x}}(f) = \frac{2\pi f}{\mathrm{c_0}} \sqrt{\varepsilon_{\mathrm{r}} - \sin^2 \theta_{\mathrm{R}}(f)}. \tag{9}$$

so that the transverse phase constant $\beta_x(f)$ must follow the next linear function with frequency to satisfy the squint-free goal condition (4):

$$\beta_{x\mathrm{GOAL}}(f) = \frac{2\pi f}{\mathrm{c_0}} \sqrt{\varepsilon_r - \sin^2 \theta_{\mathrm{GOAL}}}. \tag{10}$$

The leaky-mode dispersion is given by the transverse resonance equation (TRE)

$$\rho_0 \mathrm{e}^{-j2k_x W_1} \rho_R = 1 \tag{11}$$

where ρ_R and ρ_0 stand for the reflection coefficients at the right and left sides of the SIW of width W_1 [see Fig. 2]. Inserting (10) in (11) and taking phases, the following goal function $\Psi_{\mathrm{GOAL}}(f)$ is obtained for the phase of the reflection coefficient ρ_R, as a function of frequency and for the goal angle θ_{GOAL}, and a given width W_1:

$$\Psi_{\mathrm{GOAL}}(f) = \frac{4W_1 \pi f}{\mathrm{c_0}} \sqrt{\varepsilon_r - \sin^2 \theta_{\mathrm{GOAL}}} - \varphi_0(f, \varphi_{\mathrm{GOAL}}) + 2\pi q \tag{12}$$

where q is any integer value and φ_0 is the phase of ρ_0 which depends on frequency and the internal incidence angle φ_{INC}. As for the radiation angle θ_R, the internal angle of incidence φ_{INC} is also fixed to a goal value to keep the squint-free condition. Inserting (4) into (5) we obtain

$$\varphi_{\mathrm{INC}}(f) = \varphi_{\mathrm{GOAL}} = \arcsin \frac{\sin \theta_{\mathrm{GOAL}}}{\sqrt{\varepsilon_{\mathrm{r}}}}. \tag{13}$$

The design goal is, thus, to determine the coupled SIWs dimensions (distances between coupling vias P_i, and SIW widths W_i) which satisfy over a wideband the reflection-phase condition $\Psi_R(f) = \Psi_{\mathrm{GOAL}}(f)$, or in other words, which minimize the following error function for the reflection phases:

$$\Delta\Psi(f, W_i, \mathrm{P_i}) = \Psi_{\mathrm{GOAL}}(f, W_1) - \Psi_R(f, \mathrm{W_{i>1}}, P_i). \tag{14}$$

It is noted that the first SIW width W_1 determines the goal reflection phase Ψ_{GOAL}, while the rest of SIW widths W_i with $i > 1$ and the distance between coupling vias P_i determine the reflection phase of the right part of the circuit Ψ_R. The design methodology is described in Section III with practical examples.

TABLE I
OPTIMIZED DIMENSIONS OF COUPLED SIW LWA FOR $\theta_{\mathrm{GOAL}} = 30°$

N	SIW Width W_i (mm)	Vias Periodicity P_i (mm)
1	W_1=7.45 W_S=1.8	P_1=3.6
2a	W_1=7.37 W_2=8.27 W_S=2.52	P_1=3.76 P_2=7.75
2b	W_1=7.29 W_2=7.98 W_S=2.58	P_1=3.91 P_2=7.75
2c	W_1=7.23 W_2=7.88 W_S=2.58	P_1=4.06 P_2=7.75
3	W_1=7.19 W_2=6.93 W_3=6.9 W_S=2.99	P_1=3.57 P_2=3.29 P_3=3.37

III. DESIGN EXAMPLES

The SIW substrate is set to $H = 0.508$ mm, $\varepsilon_r = 2.2$, and the diameter of the vias is fixed to $d = 1$ mm. The row of vias at the left is set to a distance $P_0 = 2$ mm so that leakage is prevented from this side. The desired pointing angle is chosen to $\theta_{\mathrm{GOAL}} = 30°$, and the design frequency is 15 GHz. The internal incidence angle (13) is then fixed to $\varphi_{\mathrm{GOAL}} = 19°$. Sections III-A–III-C illustrate how an increased number of coupled SIWs (from $N = 1$ to $N = 3$) can be optimized to provide higher squint-free bandwidth. Table I summarizes the optimized dimensions of the five studied designs.

A. Single SIW LWA ($N = 1$)

For the single SIW LWA, the dimensions W_1, P_1, and W_S can be directly obtained as explained in [26] to achieve the desired pointing angle at the operating frequency ($\theta_{\mathrm{GOAL}} = 30°$ at 15 GHz).The values are summarized in Table I for $N = 1$. With these dimensions, Fig. 4 shows the goal reflection-phase $\Psi_{\mathrm{GOAL}}(f)$ for a squint-free response in the frequency band from 12 to 18 GHz. Also, the magnitude $|\rho_R(f)|$ and the phase $\Psi_R(f)$ of the reflection coefficient ρ_R for this $N = 1$ design are plotted. As shown in Fig. 4, the reflection-phase condition $\Psi_R(f) = \Psi_{\mathrm{GOAL}}(f)$ for leaky-mode radiation at fixed $\theta_R = 30°$ is only satisfied at a design frequency of 15 GHz. The goal reflection phase $\Psi_{\mathrm{GOAL}}(f)$ has a positive slope with frequency, which cannot be followed by the reflection phase $\Psi_R(f)$ of a single row of PRS posts, which has a negative phase gradient as shown in Fig. 4.

The frequency response for the directivity of this $N = 1$ SIW LWA design has been simulated using HFSS software for three different finite antennas of lengths $L = 16$ cm ($L = 8\lambda_0$ at 15 GHz), $L = 20$ cm, and $L = 32$ cm, all of them

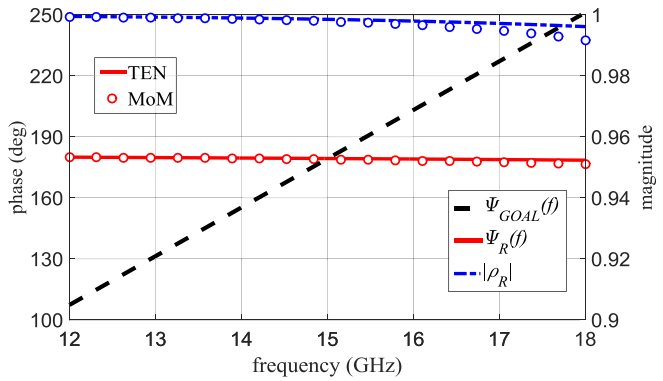

Fig. 4. Reflection coefficient for single-cavity SIW LWA with dimensions given in Table I with $N = 1$ and reflection-phase goal function for $\theta_{\text{GOAL}} = 30°$.

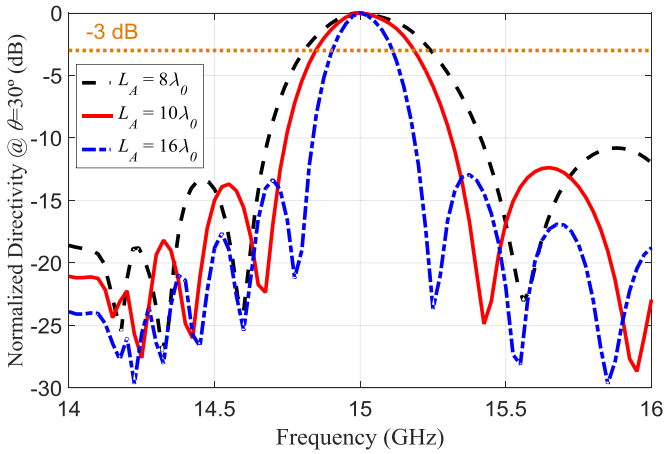

Fig. 5. Normalized directivity at $\theta = \theta_{\text{GOAL}} = 30°$ as a function of frequency of $N = 1$ SIW LWA with dimensions given in Table I for three different antenna lengths.

scanning at the desired angle $\theta = \theta_{\text{GOAL}} = 30°$ at 15 GHz. Fig. 5 represents the normalized directivity frequency response obtained in the frequency range from 14 to 16 GHz for the three antenna lengths. Due to the inherent frequency-scanning behavior of LWAs [1], a beam is scanned from near broadside ($\theta = 0°$) at low frequencies to end-fire ($\theta = 90°$) direction as frequency is increased. As a result, the frequency response of the directivity at the desired angle $\theta = \theta_{\text{GOAL}} = 30°$ shows a maximum at the design frequency of 15 GHz. The directivity at 30° drops above and below this design frequency of 15 GHz, resulting in a limited 3-dB PBW. Longer LWAs provide narrower beams (3) and higher directivities and, thus, reduced PBW, while shorter antennas result in wider beams and higher bandwidth, as shown in Fig. 5. In any case, this is the common behavior of LWAs, which limits its performance for broadband point-to-point applications as commented in the introduction of this paper.

B. Two-Coupled SIW LWA ($N = 2$)

Broadband operation with a fixed angle can be obtained if the antenna reflection phase response $\Psi_R(f)$ provides a positive phase gradient which matches $\Psi_{\text{GOAL}}(f)$ in the desired bandwidth. Similar positive phase-gradient responses

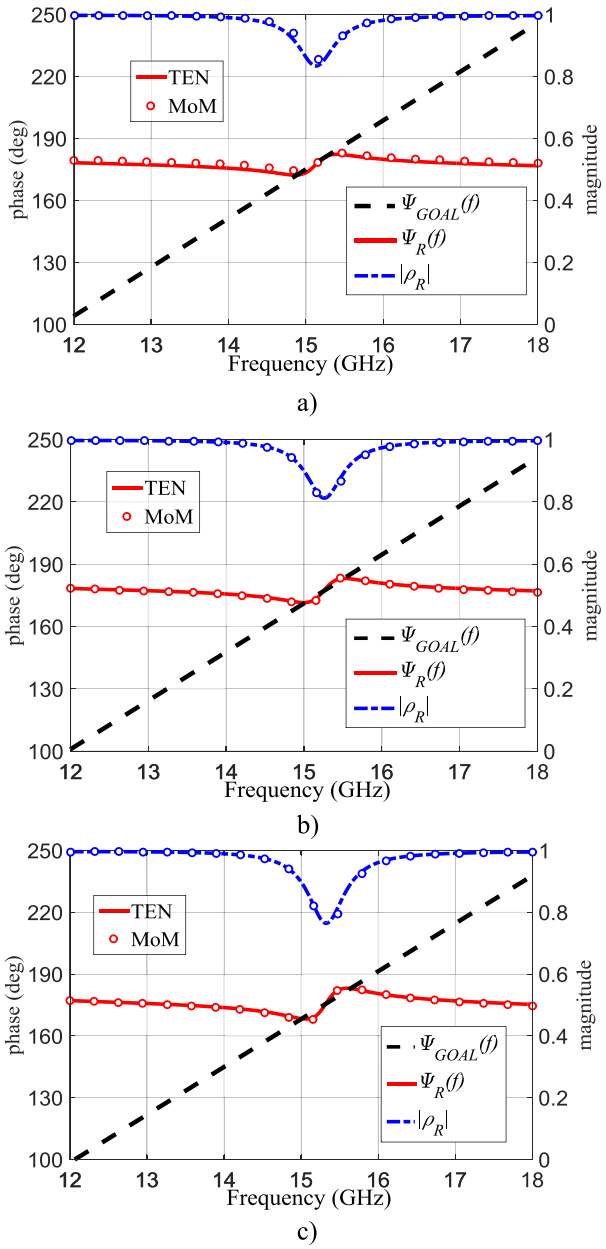

Fig. 6. Reflection coefficient for optimized coupled SIW LWA with $N = 2$ and dimensions given in Table I, and reflection-phase goal function for $\theta_{\text{GOAL}} = 30°$.

have been applied for wideband FPA radiating at broadside [19]–[25], [29]–[32]. In our case, this type of response can be obtained by inserting an extra row of vias with period P_2 which couples energy to an extra SIW of width W_2, thus leading to a coupled SIW LWA of order $N = 2$, as represented in Fig. 1(b).

This is illustrated in Fig. 6, where the reflection coefficients (magnitude and phase) for three different coupled SIW LWA designs with $N = 2$ are plotted. The coupled SIW dimensions were optimized to minimize the phase-error function (14) as explained in Section II, and they are summarized in Table I. As can be observed, the reflection phase $\Psi_R(f)$ now presents a positive slope which satisfies the squint-free condition $\Psi_R(f) = \Psi_{\text{GOAL}}(f)$ for $\theta_{\text{GOAL}} = 30°$ not only at 15 GHz,

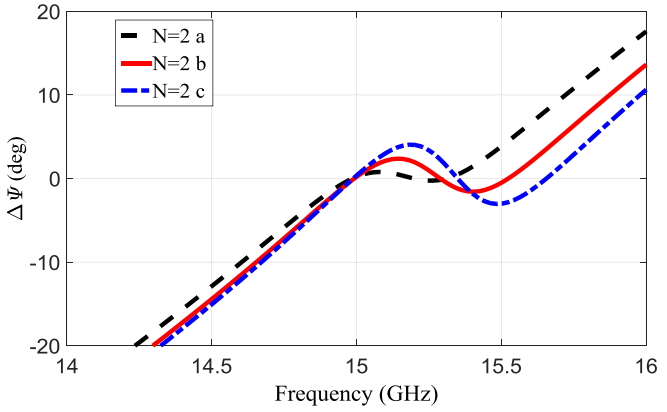

Fig. 7. Reflection-phase error function (with pointing angle $\theta_{\mathrm{GOAL}} = 30°$) for optimized coupled SIW LWA designs of Table I with $N = 2$.

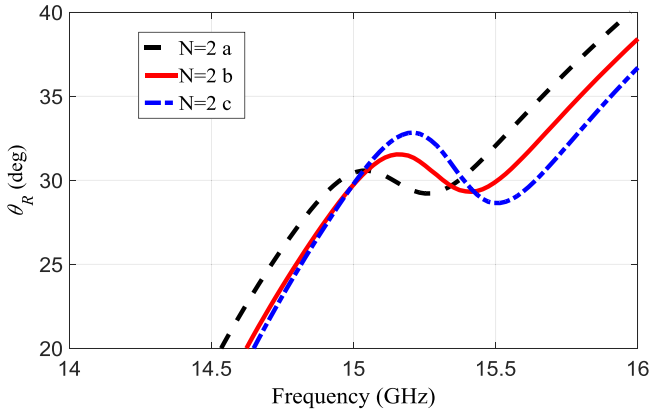

Fig. 8. Dispersion of the leaky-mode angle for optimized coupled SIW LWA designs of Table I with $N = 2$.

but in given bandwidth starting at 15 GHz and ending at 15.31 GHz for case $N = 2$a [Fig. 6(a)], 15.52 GHz for case $N = 2$b [Fig. 6(b)], and 15.65 GHz for case $N = 2$c [Fig. 6(c)]. Also, the reflection magnitude $|\rho_R(f)|$ is different to $N = 1$ case, showing a resonant behavior around the design frequency of 15 GHz.

To better compare the three different designs, the resulting phase-error functions $\Delta\Psi\ (f)$ (14) are plotted in detail in Fig. 7. It can be observed that the squint-free condition $\Delta\Psi\ (f) = 0$ is satisfied at 15 GHz, and also at two extra frequency points above, which can be distributed closer or further apart to determine the resulting squint-free bandwidth. Case $N = 2$a in Fig. 7 shows a squint-free range from 15 GHz to 15.31 GHz, case $N = 2$b from 15 to 15.52 GHz, and case $N = 2$c from 15 to 15.65 GHz.

Although one could think that more separated squint-free frequency points provide a wider free-squint bandwidth, this is not strictly true. Actually, the condition $\theta_R = \theta_{\mathrm{GOAL}} = 30°$ is guaranteed only at the $2N - 1$ frequency points where the TEN reflection-phase-error function $\Delta\Psi\ (f)$ is 0. As shown in Fig. 7, intermediate frequency points provide higher phase error as the frequency zeros are more separated (see $N = 2$c in Fig. 7). On the contrary, closer zeroes provide a flatter response of the error function (see $N = 2$a in Fig. 7). As the error function $\Delta\Psi\ (f)$ becomes higher, the condition $\theta_R = \theta_{\mathrm{GOAL}} = 30°$ is less certain and it is expected that the associated leaky-mode pointing angle θ_R to be more distant from the desired angle of 30°.

To obtain the variation with frequency of the leaky-mode pointing angle $\theta_R(f)$ with respect to the desired fixed angle θ_{GOAL}, a leaky-mode dispersion analysis must be carried out. An approximate dispersion analysis can be performed by inserting the complex reflection coefficient $\rho_R(f)$ obtained for the optimized designs (shown in Fig. 6) in (11). Then, the TRE (11) is solved for the unknown complex transverse propagation constant $k_x(f)$, from which the leaky-mode longitudinal propagation constant $k_y(f)$ can be derived using (8). Finally, from the phase constant $\beta_y(f)$, the dispersion of the angle $\theta_R(f)$ is obtained using (2). Fig. 8 shows the frequency dispersion for $\theta_R(f)$ for the three SIW LWAs designs of order $N = 2$.

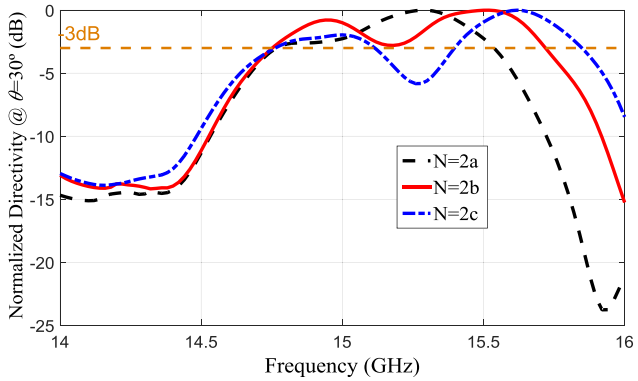

Fig. 9. Normalized directivity at $\theta = \theta_{\mathrm{GOAL}} = 30°$ as a function of frequency for optimized coupled SIW LWA designs of Table I with $N = 2$.

As expected, the three designs satisfy the condition $\theta_R = \theta_{\mathrm{GOAL}} = 30°$ at 15 GHz and at two more frequency points which correspond with the frequencies of zero phase error in Fig. 7. For intermediate frequencies, the leaky-mode pointing angle fluctuates from the goal angle of 30°, and this deviation is more pronounced for case $N = 2$c ($30° \pm 2.8°$), and less pronounced for case $N = 2$a ($30° \pm 1.5°$).

The above characteristics indicate that the design trade-offs should be applied. In particular, since the objective is to keep the LWA pointing angle to the desired angle $\theta_R = \theta_{\mathrm{GOAL}} = 30°$ and over the wider band, the trade-off relates to the location of the frequency zeros of $\Delta\Psi\ (f)$. Ultimately, this reflects to the stability of the gain/directivity at the desired beam pointing angle (30° in our case). For the three designs of order $N = 2$ (all of them with the same antenna length as for $N = 1$ design, i.e., $L = 16$ cm), the directivity at $\theta = 30°$ as obtained using HFSS is plotted in Fig. 9.

For case $N = 2$a, a 3-dB PBW from 14.75 to 15.53 GHz (780 MHz) is obtained, showing slight improvement when compared to $N = 1$ case with 430 MHz of PBW (see Fig. 5). This can be attributed to the close location of the squint-free frequency points in Fig. 8. On the contrary, case $N = 2$c showed too separated frequency zeros and too strong variation in the leaky-mode pointing angle (see Fig. 8), which results in a strong drop of directivity for intermediate frequency

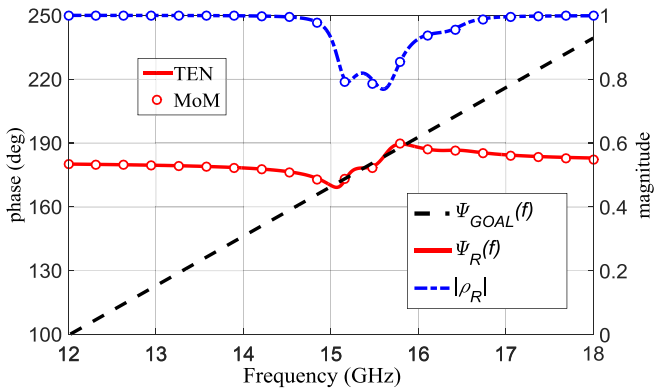

Fig. 10. Reflection coefficient for optimized coupled SIW LWA with $N = 3$ and dimensions given in Table I, and reflection-phase goal function for $\theta_{\text{GOAL}} = 30°$.

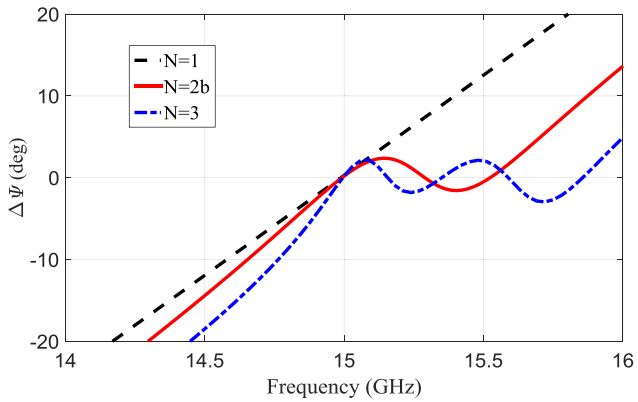

Fig. 11. Reflection-phase error function (with a goal pointing angle $\theta_{\text{GOAL}} = 30°$) for optimized coupled SIW LWA designs of Table I with $N = 1$, $N = 2$b, and $N = 3$.

points as observed in Fig. 9 around 15.25 GHz. Therefore, $N = 2$b design is the one that provides the most stable directivity response, offering a PBW of 970 MHz from 14.75 to 15.72 GHz. A tradeoff between PBW and ripple can be noticed; if lower ripple is needed, the maximum bandwidth must be reduced by locating the associated zeros to closer frequencies.

As previously commented, this numerical optimization is computationally affordable thanks to the use of closed-form expressions for all the components of the TEN. A gradient-based optimization scheme has been used to minimize the error function (12), taking 1500 simulations for convergence. To validate the results, the reflection coefficient $\rho_R(f)$ obtained with MoM is also represented with circles in Fig. 6, showing good agreement.

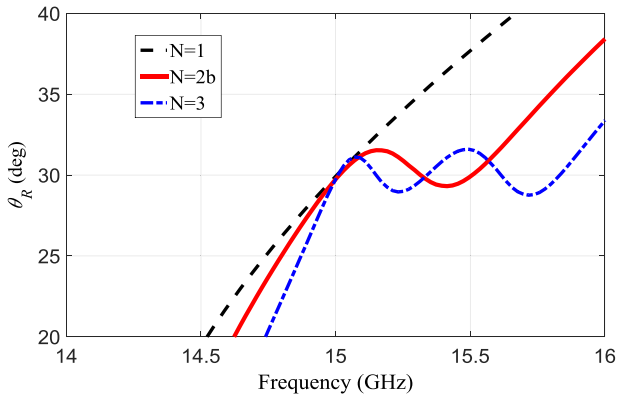

Fig. 12. Dispersion of the leaky-mode pointing angle for optimized coupled SIW LWA designs of Table I with $N = 1$, $N = 2$b, and $N = 3$.

C. Three-Coupled SIW LWA ($N = 3$)

Following a similar optimization procedure as for $N = 2$ SIW LWA, a third-order ($N = 3$) SIW LWA has been designed using the TEN, as shown in Fig. 2(d). The optimized dimensions are summarized in Table I, and the resulting reflection coefficient is plotted in Fig. 10. Again, good matching is observed between TEN and full-wave MoM results for this $N = 3$ design.

Fig. 11 shows the comparison of the phase-error function of this $N = 3$ design, with the error functions obtained for $N = 1$ and $N = 2$b. As expected, the squint-free condition $\Delta\Psi(f) = 0$ is satisfied at $2N - 1 = 5$ frequency points which can be distributed in a wider bandwidth (from 15 to 15.85 GHz) than for $N = 1$ and $N = 2$ cases.

Fig. 12 shows the comparison of the leaky-mode angle dispersion $\theta_R(f)$. The single SIW LWA ($N = 1$) shows a conventional leaky-mode dispersion [1], [5], with a pointing angle which monotonously rises with frequency. Therefore, the condition $\theta_R = \theta_{\text{GOAL}} = 30°$ can only be satisfied at one frequency point (15 GHz). However, the coupled SIW designs (with $N > 1$) present a frequency band with anomalous quasi-oscillatory stabilization of $\theta_R(f)$ around the desired pointing angle. This type of oscillatory anomalous leaky-mode dispersion was reported in [33] for a multilayer broadband FPA radiating at broadside; this is the first time it is demonstrated for an LWA pointing off-broadside.

In our case, the leaky-mode pointing angle $\theta_R(f)$ oscillates around $\theta_{\text{GOAL}} = 30°$, as shown in Fig. 12. As for $N = 2$b case, the ripples of $\theta_R(f)$ have been kept within a level of 30 ± 1.5, so that the PBW is optimized as explained in Section III-B. Case $N = 3$ presents five frequency points which satisfy $\theta_R = \theta_{\text{GOAL}} = 30°$ and are distributed in the aforementioned squint-free bandwidth from 15 to 15.85 GHz (850 MHz). This is an improvement compared to $N = 2$b design that shows a squint-free bandwidth from 15 to 15.52 GHz (520 MHz).

Finally, Fig. 13 shows the normalized gain at 30° obtained using HFSS, for the three optimized designs with $N = 1$, $N = 2$b, and $N = 3$. These full-wave results demonstrate how the gain at 30° presents a bandpass frequency response which half-power gain bandwidth increases with the number of coupled SIWs. In particular, the low-frequency limit in Fig. 13 is close to 14.5 GHz, which corresponds to the onset of the leaky mode in the coupled SIW structure for the three designs. Then, the gain rises and oscillates with low ripple (below 3 dB), and above a given upper frequency it drops. This behavior is expected according to the leaky-mode dispersion curves in Fig. 12. Table II summarizes the half-power gain frequency band and the resulting PBW for each design. It is obtained

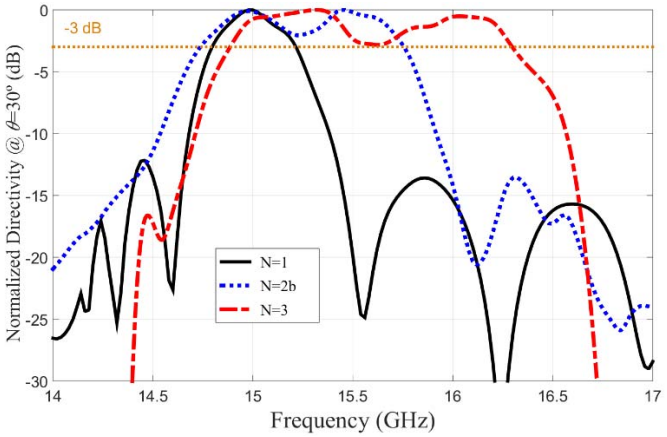

Fig. 13. Normalized gain at $\theta = \theta_{GOAL} = 30°$ as a function of frequency for optimized coupled-SIW LWA designs of Table I with $N = 1$, $N = 2b$, and $N = 3$.

TABLE II
HALF-POWER GAIN BANDWIDTH FOR DESIGNS OF TABLE I

Case	Half-power gain bandwidth at θ=30º	PBW at θ=30º	Fractional BW
N=1	14.81 GHz – 15.24 GHz	400 MHz	2.6 %
N=2b	14.75 GHz – 15.72 GHz	970 MHz	6.4 %
N=3	14.88 GHz – 16.30 GHz	1420 MHz	9.5 %

an increase of the bandwidth as the order of the coupled SIW LWA increases, from 2.6% (400 MHz) for $N = 1$ antenna, to 6.4% (970 MHz) for $N = 2b$ antenna, and finally to 9.5% (1420 MHz) for $N = 3$ SIW LWA design.

Theoretically, it is possible to synthetize more zeros in the phase-error function (14) by increasing the order of the SIW LWA, and thus cover a wider frequency band where the squint-free condition is satisfied. However, as seen in the design with two coupled SIWs, a full-wave simulation is needed to see if the ripple is lower than 3 dB and the PWB has been effectively increased. Otherwise, the dimensions of the antenna must be reoptimized and, with higher number of coupled SIWs, the process is more complicated. Therefore, we cannot establish a theoretical limitation in the order N of coupled SIW, or in the effective increase in the associated gain bandwidth, but this has to be demonstrated for each optimized design. In this paper, we have demonstrated this for $N = 1$–3.

IV. EXPERIMENTAL VALIDATION

This section presents the experimental results with manufactured prototypes of the designed antennas, which are shown in Fig. 14. All prototypes were manufactured using commercial RT-Duroid 5880 substrate ($H = 0.508$ mm, $\varepsilon_r = 2.2$, and $\tan\delta = 0.0009$). As common in this type of SIW LWAs [4], [16] and also in general SIW circuits [33], [34], a width-tapered microstrip-to-SIW transition is used for improved matching [35], [36]. Both the microstrip and the closed (nonleaky) SIW widths are linearly tapered, so that the mode conversion and matching is performed in two stages: first from

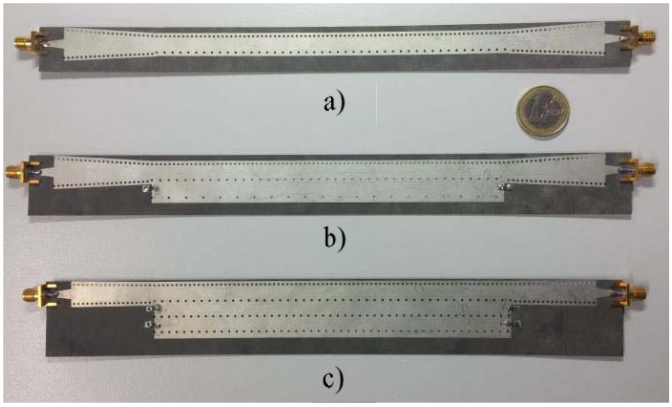

Fig. 14. Photograph of manufactured prototypes. (a) $N = 1$. (b) $N = 2b$. (c) $N = 3$.

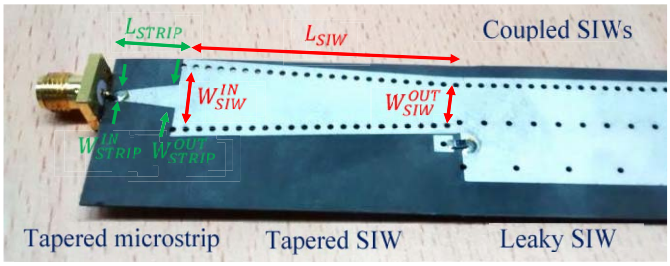

Fig. 15. Detail of microstrip-to-coupled-SIW leaky-line feeding.

TABLE III
MICROSTRIP-TO-LEAKY-SIW TRANSITION

Parameter	Dimensions	Parameter	Dimensions
W_{STRIP}^{IN}	1.62 mm	W_{SIW}^{IN}	12.40 mm
W_{STRIP}^{OUT}	4.53 mm	W_{SIW}^{OUT}	7.40 mm
L_{STRIP}	10 mm	L_{SIW}	42 mm

the TEM mode of the 50-Ω microstrip to the TE_{10} guided mode of the closed (nonleaky) SIW, and then from this guided TE_{10} mode to the quasi-TE_{10} leaky mode of the perturbed (leaky) SIW section. It is noted that matching this class of SIW LWAs is more complicated compared to other SIW components as filters [34]–[37], since SIW LWAs operate close to the cutoff frequency of the SIW mode in order to achieve leakage. As a result, the width of the radiating leaky-SIW section is very narrow, and a width-tapered SIW transition from a wider guiding input section to this narrow radiating section is requested, as reported in [4] and [16]. A detail of this feeding mechanism is illustrated in Fig. 15, and the associated widths and lengths for each section are summarized in Table III.

The measured input matching for the three prototypes is plotted in Fig. 16 together with simulated HFSS results, observing good agreement. The three coupled-SIW LWA prototypes present a cutoff frequency close to 14 GHz, where the onset of the leaky-mode radiation occurs close to broadside

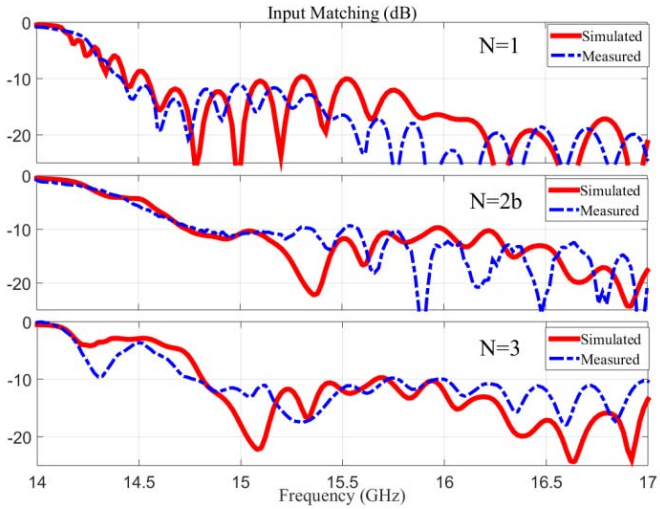

Fig. 16. Simulated and measured input matching–frequency responses for the three prototypes. (Top) $N = 1$. (Middle) $N = 2$b. (Bottom) $N = 3$.

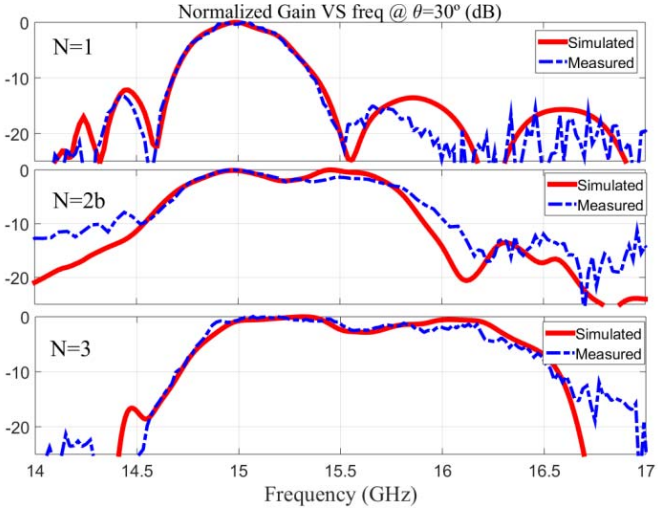

Fig. 17. Simulated and measured gain–frequency responses at the design pointing angle $\theta_{\mathrm{GOAL}} = 30°$, for the three prototypes. (Top) $N = 1$. (Middle) $N = 2$b. (Bottom) $N = 3$.

direction ($\theta \approx 0°$). As commented, it is difficult to match the structure at this cutoff frequency. This is the reason why the bandwidth improvement is designed to be at frequencies higher than 15 GHz. This way, once the microstrip-to-SIW LWA transition for one antenna is optimized, the transition for the rest will be very similar (because they will have almost the same cutoff frequency) and easier to optimize starting from the parameters of the first design. Then, as frequency increases the matching improves showing a wideband performance with reduced S_{11}. The impedance-matching bandwidth with $S_{11} < -10$ dB covers the range from 14.7 to 17 GHz for the three designs. As it can be seen in Fig. 16, the matching at lower frequencies is degraded with adding coupled SIWs. This is due to the reduced width presented by the input SIWs for higher order designs. As shown in Table I, W_1 is reduced from 7.45 mm for $N = 1$–7.29 mm for $N = 2$b and to 7.19 mm for $N = 3$. As a result, the input SIW presents higher cutoff frequency for higher-order designs, thus increasing the mismatch for lower frequencies.

However, the practical bandwidth of the antenna is limited by the aforementioned PBW for the desired pointing angle (in our case $\theta = \theta_{\mathrm{GOAL}} = 30°$). The simulated and measured frequency response of the gain at the designed angle of $\theta_{\mathrm{GOAL}} = 30°$ for the three prototypes is reported in Fig. 17.

Good agreement is observed in Fig. 17 between the simulation and experimental results, demonstrating higher PBW as the order of coupled SIWs is increased. Finally, Fig. 18 shows the comparison of the measured normalized gain frequency responses for the three manufactured prototypes, at the designed direction of $\theta = 30°$. Table IV summarizes the measured performance with taking into account the two main limiting factors in the overall SIW antennas bandwidth: the input impedance bandwidth and the PBW for the pointing angle of $\theta = 30°$.

The typical single-SIW LWA prototype shows a narrow gain bandwidth of 380 MHz at 15 GHz (i.e., 2.5% fractional PBW), due to the well-known frequency-beam squint associated with common SIW LWAs. The peak gain of this antenna is

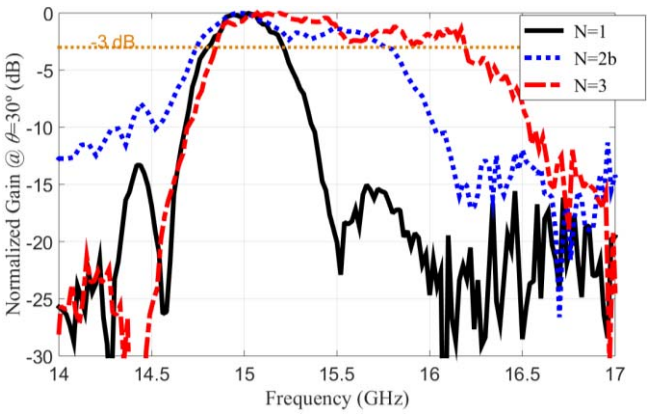

Fig. 18. Measured normalized gain versus frequency response at angle $\theta_{\mathrm{GOAL}} = 30°$, for the three prototypes. $N = 1$, $N = 2$b, and $N = 3$.

12.8 dBi, produced at a frequency of 15 GHz, with an aperture length of $L = 16$ cm $= 8\lambda_0$ at 15 GHz, with a directivity of 13.9 dBi, and a radiation efficiency of 77.6%. The proposed new design with $N = 3$ coupled SIWs demonstrate a superior performance, with a PBW of 1360 MHz and a peak gain of 11.2 dBi, produced at 15.2 GHz (and similar radiation efficiency of 77.7% for a lower directivity of 12.3 dBi). As usually happens, there is a tradeoff between the gain and the bandwidth. In our case, this is translated into a 1.6-dB drop in gain and directivity, for an improvement of 3.6 times of the associated PBW (from 380 to 1360 MHz, i.e., from 2.5% to 9% fractional bandwidth).

The directivity reduction for higher order N can be attributed to lower aperture efficiency created by the interaction of multiple coupled leaky modes, which can radiate at different angles. This can be observed in the measured radiation patterns shown in Fig. 19. Effectively, while $N = 1$ order LWA design shows the typical single-scanned beam pattern, higher order designs produce several peaks in the H-plane radiation patterns, which might be distributed at different scanning

TABLE IV

ELECTROMAGNETIC PERFORMANCE OF PROTOTYPES

Case	Impedance Bandwidth (GHz) (S11<-10dB)	half-power gain bandwidth at θ=30º (GHz)	Peak Directivity (dBi)	Peak Gain (dBi)
N=1	14.42–17	14.82–15.20	13.9	12.8
N=2b	14.79–17	14.76–15.76	12.5	11.5
N=3	14.78–17	14.84–16.20	12.3	11.2

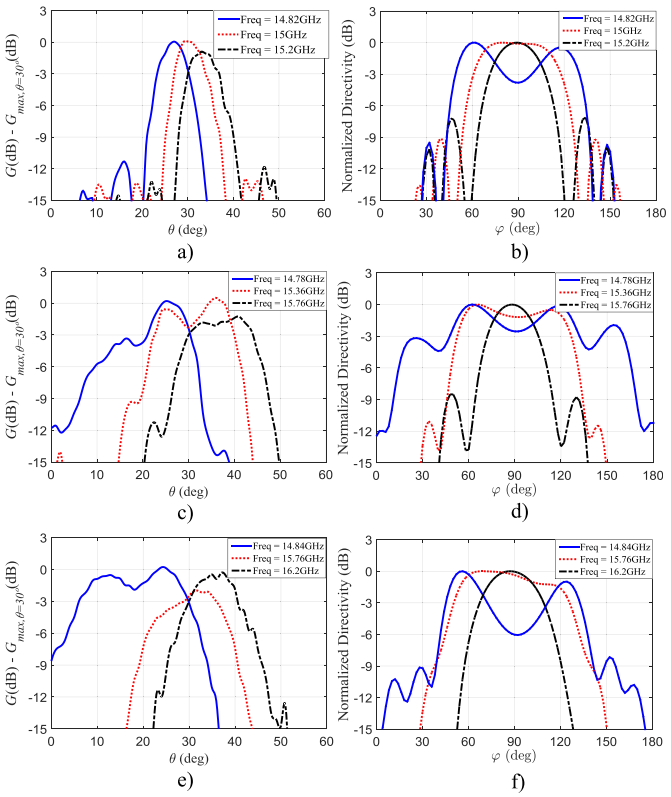

Fig. 19. Measured H-plane radiation patterns ($\varphi = 90°$) for different frequencies in the designed antennas bandwidth. (a) $N = 1$. (c) $N = 2$b. (e) $N = 3$. Measured E-plane radiation patterns ($\theta = 30°$). (b) $N = 1$. (d) $N = 2$b. (f) $N = 3$.

angles [see for instance the evident formation of two peaks in $N = 2$b design at 15.36 GHz in Fig. 19(c)]. Obviously, this reduces the associated antenna directivity. However, it is indeed the contribution of different leaky modes to radiation at the desired angle $\theta = 30°$ for different frequencies, what makes the resulting gain bandwidth to increase for this angle for higher order N designs. The radiation patterns have been plotted for three frequencies inside the PBW of each design. They are normalized to the maximum gain, so that it is easy to observe that in the upper and lower frequencies inside the PBW for each design, a 3-dB drop in the gain occurs at the angle $\theta = 30°$. Also, the respective E-plane patterns (for $\theta = 30°$) are shown in Fig. 19, showing the typical fan beam which is less directive in this plane perpendicular to the antenna.

squint-free LWAs

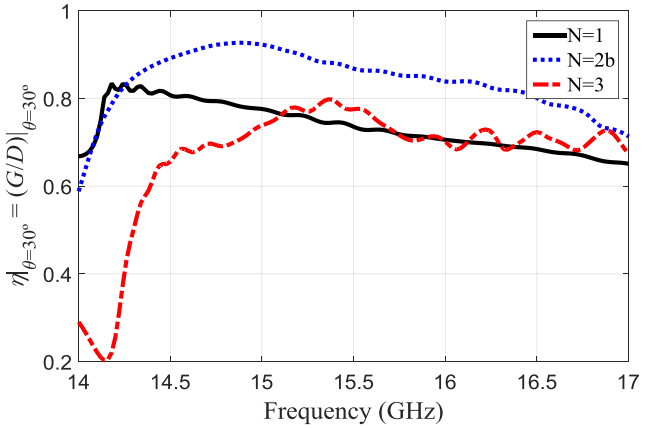

Fig. 20. Radiation efficiency for the three SIW LWA designs of order $N = 1$, $N = 2$b, and $N = 3$ at $\theta = 30°$ from 14 to 17 GHz.

On the other hand, the variation of the radiation efficiency with frequency for the three designed antennas is depicted in Fig. 20. It must be observed again that this radiation efficiency is understood as the relation between the directivity and the gain at the angle of interest $\theta = 30°$. This efficiency evaluates how efficiently the power is being radiated to this design angle $\theta = 30°$ at any frequency inside the antenna bandwidth. As it can be seen, the three designs present efficiency values over 60% in all the bandwidth.

V. CONCLUSION

It has been demonstrated that by suitably coupling leaky SIW lines, the beam-squint effect associated with directive SIW LWAs can be reduced, obtaining a wider gain bandwidth for a designed elevation angle. The proposed coupled-SIW LWA topology maintains the planar, single feeding, and passive properties of SIW LWAs. The structure is extremely integrated, thanks to the use of longitudinally coupled SIW guides along the antenna length. In this way, it avoided the use of bulky 3-D lenses, non-Foster active arrays, or more complicated nonreciprocal structures reported in the previous squint-free LWAs technologies.

The TEN used to design this wideband SIW LWA, suggests that coupled-cavity filter synthesis techniques could be applied for a systematic design of this type of planar high-gain SIW antennas with application for broadband point-to-point wireless communications.

REFERENCES

[1] A. A. Oliner and D. R. Jackson, "Leaky-wave antennas," in *Antenna Engineering Handbook*, 4th ed., J. L. Volakis, Ed. New York, NY, USA: McGraw-Hill, 2007, ch. 11.

[2] A. Sanada, H. Kubo, S.-I. Matsuzawa, and K. Sato, "Automotive radar antenna application using balanced composite right/left-handed metamaterials," in *Proc. Antennas Propag. Soc. Int. Symp.*, Jul. 2006, pp. 398–401.

[3] M. Ettorre, A. Neto, G. Gerini, and S. Maci, "Leaky-wave slot array antenna fed by a dual reflector system," *IEEE Trans. Antennas Propag.*, vol. 56, no. 10, pp. 3143–3149, Oct. 2008.

[4] Y. J. Cheng, W. Hong, K. Wu, and Y. Fan, "Millimeter-wave substrate integrated waveguide long slot leaky-wave antennas and two-dimensional multibeam applications," *IEEE Trans. Antennas Propag.*, vol. 59, no. 1, pp. 40–47, Jan. 2011.

[5] J. L. Gómez-Tornero, F. Quesada-Pereira, A. Alvarez-Melcón, G. Goussetis, A. R. Weily, and Y. J. Guo, "Frequency steerable two dimensional focusing using rectilinear leaky-wave lenses," *IEEE Trans. Antennas Propag.*, vol. 59, no. 2, pp. 407–415, Feb. 2011.
[6] A. Neto, S. Bruni, G. Gerini, and M. Sabbadini, "The leaky lens: A broad-band fixed-beam leaky-wave antenna," *IEEE Trans. Antennas Propag.*, vol. 53, no. 10, pp. 3240–3246, Oct. 2005.
[7] A. Neto, "UWB, non dispersive radiation from the planarly fed leaky lens antenna—Part 1: Theory and design," *IEEE Trans. Antennas Propag.*, vol. 58, no. 7, pp. 2238–2247, Jul. 2010.
[8] C. Caloz, S. Abielmona, H. Nguyen, and A. Rennings, "Dual composite right/left-handed (D-CRLH) leaky-wave antenna with low beam squinting and tunable group velocity," *Phys. Status Solidi B*, vol. 244, no. 4, pp. 1219–1226, 2007.
[9] M. A. Antoniades and G. V. Eleftheriades, "A CPS leaky-wave antenna with reduced beam squinting using NRI-TL metamaterials," *IEEE Trans. Antennas Propag.*, vol. 56, no. 3, pp. 708–721, Mar. 2008.
[10] N. Nasimuddin, Z. N. Chen, and X. Qing, "Substrate integrated metamaterial-based leaky-wave antenna with improved boresight radiation bandwidth," *IEEE Trans. Antennas Propag.*, vol. 61, no. 7, pp. 3451–3457, Jul. 2013.
[11] K. M. Kossifos and M. A. Antoniades, "Analysis of an off-broadside zero beam-squinting leaky-wave antenna using metamaterials," in *Proc. 18th Medit. Electrotech. Conf. (MELECON)*, Lemesos, Cyprus, 2016, pp. 1–4.
[12] A. Shahvarpour, A. A. Melcon, and C. Caloz, "Bandwidth enhancement and beam squint reduction of leaky modes in a uniaxially anisotropic meta-substrate," in *Proc. IEEE Int. Symp. Antennas Propag.*, Jul. 2010, pp. 1–4.
[13] A. Porokhnyuk, T. Ueda, Y. Kado, and T. Itoh, "Nonreciprocal metamaterial for non-squinting leaky-wave antenna with enhanced beam steering," in *Proc. IEEE Int. Symp. Antennas Propag.*, Jul. 2013, pp. 2289–2290.
[14] D. F. Sievenpiper, "Superluminal waveguides based on non-foster circuits for broadband leaky-wave antennas," *IEEE Antennas Wireless Propagat. Lett.*, vol. 10, pp. 231–234, 2011.
[15] D. Muha, S. Hrabar, I. Krois, I. Bonić, A. Kiričenko, and D. Zaluški, "Design of microstrip non-foster leaky-wave antenna," in *Proc. 21st Int. Conf. Appl. Electromag. Commun. (ICECom)*, Dubrovnik, Croatia, 2013, pp. 1–3.
[16] A. J. Martínez-Ros, J. L. Gómez-Tornero, and G. Goussetis, "Planar leaky-wave antenna with flexible control of the complex propagation constant," *IEEE Trans. Antennas Propag.*, vol. 60, no. 3, pp. 1625–1630, Mar. 2012.
[17] J. L. Gómez-Tornero, A. Martínez-Ros, A. Álvarez-Melcón, F. Mesa, and F. Medina, "Substrate integrated waveguide leaky-wave antenna with reduced beam squint," in *Proc. Eur. Microw. Conf. (EuMC)*, Nuremberg, Germany, 2013, pp. 491–494.
[18] J. L. Gómez-Tornero, M. Poveda-García, R. Guzmán-Quirós, and D. Cañete-Rebenaque, "Reducing the beam squint in scanned leaky-wave antennas using coupled SIW cavities," in *Proc. IEEE Int. Symp. Antennas Propag. (APSURSI)*, Jun. 2016, pp. 77–78.
[19] A. P. Feresidis and J. C. Vardaxoglou, "A broadband high-gain resonant cavity antenna with single feed," in *Proc. EuCAP*, Nice, France, 2006, pp. 1–5.
[20] M. A. Al-Tarifi, D. E. Anagnostou, A. K. Amert, and K. W. Whites, "Bandwidth enhancement of the resonant cavity antenna by using two dielectric superstrates," *IEEE Trans. Antennas Propag.*, vol. 61, no. 4, pp. 1898–1908, Apr. 2013.
[21] C. Mateo-Segura, A. P. Feresidis, and G. Goussetis, "Bandwidth enhancement of 2-D leaky-wave antennas with double-layer periodic surfaces," *IEEE Trans. Antennas Propag.*, vol. 62, no. 2, pp. 586–593, Feb. 2014.
[22] K. Konstantinidis, K. P. Feresidis, and P. S. Hall, "Multilayer partially reflective surfaces for broadband Fabry–Pérot cavity antennas," *IEEE Trans. Antennas Propag.*, vol. 62, no. 7, pp. 3474–3481, Jul. 2014.
[23] K. Konstantinidis, A. P. Feresidis, and P. S. Hall, "Broadband subwavelength profile high-gain antennas based on multi-layer metasurfaces," *IEEE Trans. Antennas Propag.*, vol. 63, no. 1, pp. 423–427, Jan. 2015.
[24] B. P. Chacko, G. Augustin, and T. A. Denidni, "FPC Antennas : C-band point-to-point communication systems." *IEEE Antennas Propag. Mag.*, vol. 58, no. 1, pp. 56–64, Feb. 2016.
[25] A. Chaabane, F. Djahli, H. Attia, L. M. Abdelghani, and T. A. Denidni, "Wideband and high-gain EBG resonator antenna based on dual layer PRS," *Microw. Opt. Technol. Lett.*, vol. 59, pp. 98–101, Jan. 2017.
[26] A. J. Martínez-Ros, J. L. Gómez-Tornero, and F. Quesada-Pereira, "Efficient analysis and design of novel SIW leaky-wave antenna," *IEEE Antennas Wireless Propag. Lett.*, vol. 12, pp. 496–499, 2013.
[27] N. Marcuvitz, "Inductive post," in *Waveguide Handbook*. London, U.K.: Peregrinus, 1986, pp. 285–289.
[28] E. F. Kuester, R. T. Johnk, and D. C. Chang, "The thin-substrate approximation for reflection from the end of a slab-loaded parallel-plate waveguide with application to microstrip patch antennas," *IEEE Trans. Antennas Propag.*, vol. AP-30, no. 5, pp. 910–917, Sep. 1982.
[29] Y. Ge, K. P. Esselle, and T. S. Bird, "The use of simple thin partially reflective surfaces with positive reflection phase gradients to design wideband, low-profile EBG resonator antennas," *IEEE Trans. Antennas Propag.*, vol. 60, no. 2, pp. 743–750, Feb. 2012.
[30] B. A. Zeb, Y. Ge, K. P. Esselle, Z. Sun, and M. E. Tobar, "A simple dual-band electromagnetic band gap resonator antenna based on inverted reflection phase gradient," *IEEE Trans. Antennas Propag.*, vol. 60, no. 10, pp. 4522–4529, Oct. 2012.
[31] N. Wang, Q. Liu, C. Wu, L. Talbi, Q. Zeng, and J. Xu, "Wideband Fabry–Pérot resonator antenna with two complementary FSS layers," *IEEE Trans. Antennas Propag.*, vol. 62, no. 5, pp. 2463–2471, May 2014.
[32] A. Hosseini, F. Capolino, and D. R. Jackson, "Leaky-wave explanation of gain-bandwidth-enhanced Fabry–Pérot Cavity antennas formed by a thick multilayer partially-reflective surface," in *Proc. Antennas Propag. Soc. Int. Symp.*, Vancouver, BC, Canada, Jul. 2015, pp. 1090–1091.
[33] D. Deslandes and K. Wu, "Integrated microstrip and rectangular waveguide in planar form," *IEEE Microw. Wireless Compon. Lett.*, vol. 11, no. 2, pp. 68–70, Feb. 2001.
[34] D. Deslandes and K. Wu, "Single-substrate integration technique of planar circuits and waveguide filters," *IEEE Trans. Microw. Theory Tech.*, vol. 51, no. 2, pp. 593–596, Feb. 2003.
[35] D. Deslandes, "Design equations for tapered microstrip-to-substrate integrated waveguide transitions," in *IEEE MTT-S Int. Microw. Symp. Dig.*, May 2010, pp. 704–707.
[36] E. Miralles, H. Esteban, C. Bachiller, A. Belenguer, and V. E. Boria, "Improvement for the design equations for tapered microstrip-to-substrate integrated waveguide transitions," in *Proc. Int. Conf. Electromagn. Adv. Appl.*, Sep. 2011, pp. 652–655.
[37] G. Matthaei, L. Young, and E. M. T. Jones, *Microwave Filters, Impedance-Matching Networks, and Coupling Structures*. New York, NY, USA: McGraw-Hill, 1965.

Miguel Poveda-García was born in Pozohondo, Spain, in 1992. He received the telecommunications engineering degree and master's degree in telecommunications engineering from the Technical University of Cartagena, Cartagena, Spain, in 2014 and 2016, respectively, where he is currently pursuing the Ph.D. degree with a focus on the analysis of the dispersion of planar leaky-wave antennas in substrate-integrated waveguide technology and their design for different applications.

His current research interests include leaky-wave antennas and their application in telecommunication systems, Internet of Things, and energy harvesting.

David Cañete-Rebenaque was born in Valencia, Spain, in 1976. He received the telecommunications engineering degree from the Technical University of Valencia, Valencia, in 2000, and the Ph.D. degree from the Technical University of Cartagena, Cartagena, Spain, in 2009.

In 2001, he joined the Mobile Communication Company, as an RF Engineer. In 2002, he joined the Communications and Information Technologies Department, Technical University of Cartagena, where he is involved in research and teaching activities. His current research interests include the analysis and design of microwave circuits and antennas.

George Goussetis (S'99–M'02–SM'12) received the diploma degree in electrical and computer engineering from the National Technical University of Athens, Athens, Greece, in 1998, the B.Sc. degree (Hons.) in physics from University College London, London, U.K., in 2002, and the Ph.D. degree from the University of Westminster, London, U.K., in 2002.

In 1998, he joined the Space Engineering, Rome, Italy, as an RF Engineer. In 1999, he joined the Wireless Communications Research Group, University of Westminster, as a Research Assistant. From 2002 to 2006, he was a Senior Research Fellow with Loughborough University, Loughborough, U.K. From 2006 to 2009, he was a Lecturer and an Assistant Professor with Heriot-Watt University, Edinburgh, U.K., where he joined as a Reader in 2013, and then became a Professor in 2014. From 2009 to 2013, he was a Reader and an Associate Professor with Queen's University Belfast, Belfast, U.K. He has authored or co-authored over 400 peer-reviewed papers 5 book chapters and 1 book, and holds 4 patents. His current research interests include microwave and antenna components and subsystems.

Dr. Goussetis was a co-recipient of the 2011 European Space Agency Young Engineer of the Year Prize, the 2011 EuCAP Best Student Paper Prize, the 2012 EuCAP Best Antenna Theory Paper Prize, and the 2016 Bell Labs Prize. He held a research fellowship with the Onassis Foundation in 2001, U.K. Royal Academy of Engineering from 2006 to 2011, and European Marie-Curie in 2011–2012 and again in 2014–2017. He serves as an Associate Editor for IEEE ANTENNAS AND WIRELESS PROPAGATION LETTERS.

José Luis Gómez-Tornero (S'01–M'06–SM'14) was born in Murcia, Spain, in 1977. He received the telecommunications engineering degree from the Polytechnic University of Valencia, Valencia, Spain, in 2001, and the Laurea (Ph.D.) degree (*cum laude*) in telecommunication engineering from the Technical University of Cartagena (UPCT), Cartagena, Spain, in 2005.

In 2000, he joined the Radio Frequency Division, Industry Alcatel Espacio, Madrid, Spain, where he was involved in the development of microwave active circuits for telemetry, tracking, and control transponders for space applications. In 2001, he joined with the UPCT, where he has been an Associate Professor since 2008, and was also a Vice Dean for Students and Lectures affairs as a faculty member of telecommunication engineering. He was a Visiting Researcher/Professor with the University of Loughborough, Loughborough, U.K., Heriot-Watt University, Edinburgh, U.K., Queen's University of Belfast, Belfast, U.K., and CSIRO ICT Center, Sydney, NSW, Australia. In 2010, he was appointed as a CSIRO Distinguished Visiting Scientist by the CSIRO ICT Center. He has co-authored over 50 peer-reviewed journal papers and 100 conference papers. His current research interests include the development of numerical methods for the analysis and design of leaky-wave devices in planar and waveguide technologies, their application for telecoms, RF identification/localization, microwave heating/sensing, wireless power transmission/harvesting, hyperthermia, and analog signal processing, and the innovation in the area of higher education teaching/learning.

Dr. Gómez-Tornero was a recipient of the National Award from the foundation EPSON-Ibérica for the best Ph.D. project in the field of technology of information and communications in 2004 and the Vodafone Foundation Award for the best Spanish Ph.D. thesis in the area of advanced mobile communications technologies in 2006. He was a co-recipient of the 2010 IEEE Engineering Education Conference Award, the 2011 EuCAP Best Student Paper Prize, the 2012 EuCAP Best Antenna Theory Paper Prize, the 2012 and 2013 Spanish URSI Prize for the Best Student Paper, and the 2018 iWAT Best Poster Award. His thesis was also awarded the Best Thesis in the area of electrical engineering by the Technical University of Cartagena, in 2006. His Ph.D. students' theses received the 2014 Hispasat Prize and the 2015 Hisdesat Prize for the best Ph.D. thesis in Satellite Communication Technologies.